Consistency of atomic data for the interpretation of beam emission spectra

2010 Plasma Phys. Control. Fusion 52 125008

(http://iopscience.iop.org/0741-3335/52/12/125008)

Plasma Phys. Control. Fusion **52** (2010) 125008 (17pp) doi:10.1088/0741-3335/52/12/125008

Consistency of atomic data for the interpretation of beam emission spectra

E Delabie[1], M Brix[2], C Giroud[2], R J E Jaspers[3], O Marchuk[4], M G O'Mullane[5], Yu Ralchenko[6], E Surrey[2], M G von Hellermann[1], K D Zastrow[2] and JET-EFDA Contributors[7]

JET-EFDA Culham Science Centre, Abingdon, OX14 3DB, UK
[1] FOM Institute for Plasma Physics Rijnhuizen, Association EURATOM-FOM, PO Box 1207, 3430 BE Nieuwegein, The Netherlands
[2] EURATOM/CCFE Association, Culham Science Centre, Abingdon, OX14 3DB, UK
[3] Eindhoven University of Technology, Postbus 513, 5600 MB Eindhoven, The Netherlands
[4] Forschungszentrum Juelich, Association EURATOM-FZJ, 52425, Juelich, Germany
[5] Department of Physics, University of Strathclyde, 107 Rottenrow, Glasgow G4 0NG, UK
[6] Atomic Physics Division, National Institute of Standards and Technology, Gaithersburg, MD 20899-8422, USA

E-mail: e.delabie@fz-juelich.de

Received 27 August 2010, in final form 8 October 2010
Published 8 November 2010
Online at stacks.iop.org/PPCF/52/125008

Abstract

Several collisional–radiative (CR) models (Anderson *et al* 2000 *Plasma Phys. Control. Fusion* **42** 781–806, Hutchinson 2002 *Plasma Phys. Control. Fusion* **44** 71–82, Marchuk *et al* 2008 *Rev. Sci. Instrum.* **79** 10F532) have been developed to calculate the attenuation and the population of excited states of hydrogen or deuterium beams injected into tokamak plasmas. The datasets generated by these CR models are needed for the modelling of beam ion deposition and (excited) beam densities in current experiments, and the reliability of these data will be crucial to obtain helium ash densities on ITER combining charge exchange and beam emission spectroscopy. Good agreement between the different CR models for the neutral beam (NB) is found, if corrections to the fundamental cross sections are taken into account. First the H_α and H_β beam emission spectra from JET are compared with the expected intensities. Second, the line ratios within the Stark multiplet are compared with the predictions of a sublevel resolved model. The measured intensity of the full multiplet is ≈30% lower than expected on the basis of beam attenuation codes and the updated beam emission rates, but apart from the atomic data this could also be due to the characterization of the NB path and line of sight integration and the absolute calibration of the optics. The modelled $n = 3$ to $n = 4$ population agrees very well with the ratio of the measured H_α to H_β beam emission intensities.

[7] See the appendix of F Romanelli *et al* 2008 *Proc. 22nd IAEA Fusion Energy Conf. (Geneva, Switzerland)*.

Good agreement is found as well between the NB power fractions measured with beam emission in plasma and on the JET Neutral Beam Test Bed. The Stark line ratios and σ/π intensity ratio deviate from a statistical distribution, in agreement with the CR model in parabolic states from Marchuk *et al* (2010 *J. Phys. B: At. Mol. Opt. Phys.* **43** 011002).

(Some figures in this article are in colour only in the electronic version)

1. Motivation

Powerful neutral hydrogen or deuterium beams provide the dominant external heating and momentum input in most large scale tokamak experiments. For the interpretation of neutral beam (NB) heated discharges, detailed knowledge is required about the energy distribution of the neutrals (power fractions) and the attenuation of the beams in order to obtain radial profiles of the fast ion deposition and hence of the heating, torque and beam driven current. For the quantitative interpretation of charge exchange (CX) spectra, the local NB fluxes and population of excited states in the beam are needed to convert CX emissivities into local impurity densities. All these calculations strongly rely on the accuracy of the atomic data for the NB that is provided by collisional–radiative (CR) models of the beam [1–3, 5, 6].

When the beam emission spectrum (BES) was recorded for the first time, it was immediately proposed to monitor the beam attenuation, and hence the accuracy of the effective beam stopping cross sections, using the observed beam emission intensities [7, 8]. This replaces the accumulated error on the beam attenuation along the beam path [9], by a local error in the beam emission rate. Beam emission, when combined with charge exchange recombination spectroscopy (CXRS), also has the potential of reducing the need of an absolute calibration of the CXRS spectra and a calculation of the intersection integral between a line of sight and the NB, to a relative calibration between several spectral bands [8, 10, 11]. The combination of BES and CXRS is the only feasible method to measure helium ash concentrations with the requested accuracy on ITER where only a small fraction ($\approx$1%) of the diagnostic beam reaches the plasma centre and where calibrations of the tokamak side optics on a regular basis will be impossible [12]. The beam emission intensity and Doppler shift are also widely used to characterize the beam (power fractions [9, 13, 14], alignment [15], divergence [14]).

Apart from using the intensity of the full BES multiplet, the σ/π intensity ratio [9, 12, 16, 17] and Stark splitting [18, 19] can be used as an alternative to polarization based motional Stark effect (MSE) diagnostics, as proposed for the ITER diagnostic and heating beam, respectively. For these applications the Stark level population structure of the beam neutrals is required to model the spectra, like for polarization based MSE diagnostics when σ- and π-lines overlap.

Despite these promising applications, the use of beam emission has been hampered by the reliability of the involved atomic data and the complexity of the spectra. At the same time, the modelled NB fast ion deposition has been exploited at ever higher accuracy, thereby strongly relying on the accuracy of the underlying beam stopping calculations. It is the aim of this paper to check the consistency of the various beam modelling efforts and to quantitatively compare modelled NB densities with measured beam densities from beam emission on JET.

In section 2 several published CR models for the NB are compared. A distinction is made between models that implicitly assume a statistical population of the Stark levels within an n-shell (sections 2.1–2.3) and models that have Stark level resolution (section 2.4). The

latter models are mainly useful for the analysis of MSE data. In section 3 measured beam emission intensities from JET are compared with the expected beam densities from the beam stopping calculations. The expected line ratios within the MSE multiplet are compared with experimental data in section 4.

2. Atomic models of the NB

2.1. CR models for the NB (n-resolved)

The first NB models that take excited states into account are by Boley *et al* [20] and Janev *et al* [5]. The focus of these works was solely on the penetration length of NBs. Although beam stopping is mainly determined by direct proton impact ionization and CX from the ground state, excited states become increasingly important with increasing beam energy and plasma density. Seraydarian *et al* [7] found relatively good agreement between the measured and predicted beam emission intensity on DIII-D, using a model based on the data of Boley *et al* [20]. However, the ion impact excitation cross sections used in [20] were too large, which makes the interpretation of the beam emission results in [7] difficult. Mandl *et al* [9] compared the measured and expected beam densities on JET using the ADAS CR model (here referred to as ADAS89). They found relatively good agreement between model and experiment. Anderson *et al* [1] thoroughly revisited the ADAS beam model (here referred to as ADAS97) and brought it to a large extent in line with the 1993 review of atomic data by Janev and Smith [21]. The observed intensity on JET was found to be 30% lower than predicted. Hutchinson [2] built a CR model of the beam based on the Janev 1989 and 1993 atomic datasets [5, 21] and found a large discrepancy with ADAS97. Marchuk *et al* [3] assessed the atomic data needs for active beam spectroscopy on ITER (based on the Janev 1993 dataset) and found good agreement between their CR model and ADAS97, but only compared for the ITER diagnostic beam relevant conditions of 100 keV/amu.

2.2. Consistency of atomic data for NB emission

An investigation of the discrepancies between the CR models [1–3] revealed two issues: (1) the high energy part of the proton impact ionization cross section for excited states published in the Janev 1993 review is based on erroneous input data from [22]. Although this error was noted [23, 24] and corrected by the authors [25], the IAEA recommended data in the Alladin database [26] have not changed yet. A new fit to the ionization cross sections has been made and implemented in the CR models of ADAS (see [27] for details) and Marchuk *et al*. The different datasets are compared in figure 1. (2) Furthermore, a bug in the ADAS CR code affected the CX cross sections for excited donor states in hydrogen, strongly affecting the beam emission rates below 100 keV/amu. The corrected dataset will here be referred to as ADAS10.[8] The result of these corrections is visually depicted in figure 2. Both the corrected emission rates of ADAS, Marchuk *et al* and Hutchinson agree within 5% for the plasma and beam conditions studied here. The measured beam densities derived from these beam emission rates will be compared with the experimental data from JET in section 3.

2.3. Consistency of atomic data for NB stopping

The changes mentioned above in the electron loss cross sections from excited states in the NB, and the corresponding uncertainties, have only a small influence on the NB stopping

[8] These data are a part of ADAS release v3.1.

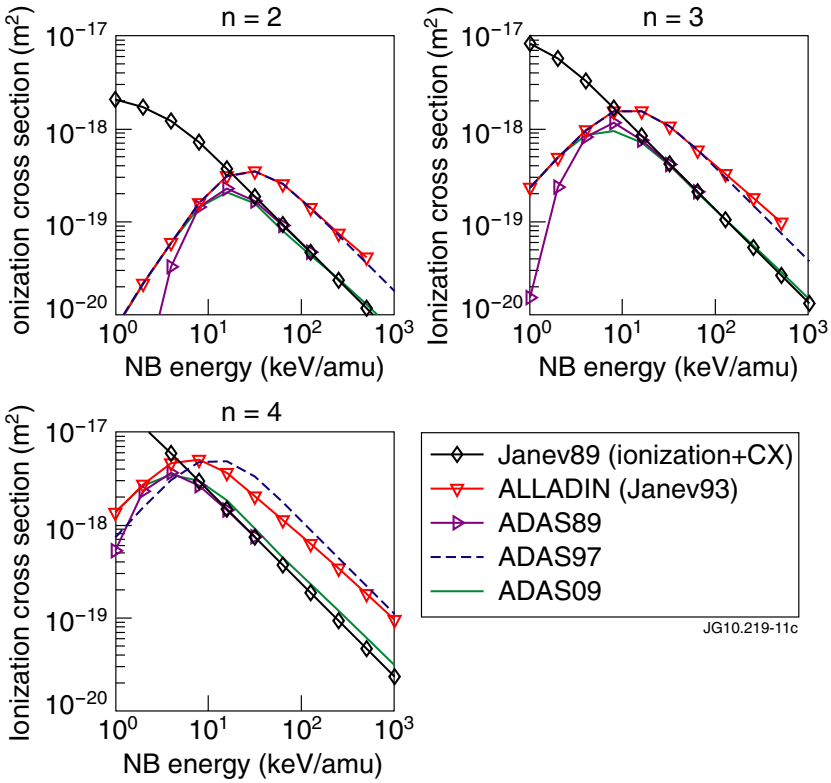

Figure 1. Proton impact ionization of excited states of the hydrogen atom. Recommended datasets (Janev89 [5] and Janev93 (as in the ALLADIN database) [21, 26]) and data used in the ADAS beam emission models are shown.

cross sections for current experiments. This is because excited states only contribute ≈20% to the effective beam stopping cross section for JET-like beams and plasmas (50 keV/amu, $n_e = 5 \times 10^{19}\,m^{-3}$). For ITER-like beams (500 keV/amu, $n_e = 1 \times 10^{20}\,m^{-3}$), however, this augments to ≈45%. The models used here do not take ionization by the Lorentz field into account, which is negligible for present experimental conditions but could increase the ionization through excited states even further for the ITER heating beams. In figure 3(*a*) the increase in the beam stopping cross section due to stepwise ionization is shown as a function of electron density for several NB energies. In figure 3(*b*) beam stopping cross sections from several datasets are compared. The difference between the beam stopping cross sections from ADAS and Marchuk *et al* [3] is in all conditions below a few per cent. The analytical expressions for the beam stopping cross sections provided by Suzuki *et al* [6] are on average 10% higher for current experimental conditions. The 1989 effective beam stopping data from Janev *et al* [5], which is based on outdated data compared with the 1993 review by Janev and Smith [21] and is not shown here, is higher by more than 20% but merges with the current data at beam energies of several 100 keV/amu. The change between the ADAS10 and ADAS97 beam stopping cross sections is also plotted. The difference stays below 5%. In conclusion, the different sets of beam stopping data for deuterium plasmas [1, 3, 6] only show a small deviation and are for current experimental conditions dominated by ion impact ionization and CX from the ground state. Changes in the excited population (e.g. ADAS97 versus ADAS10)

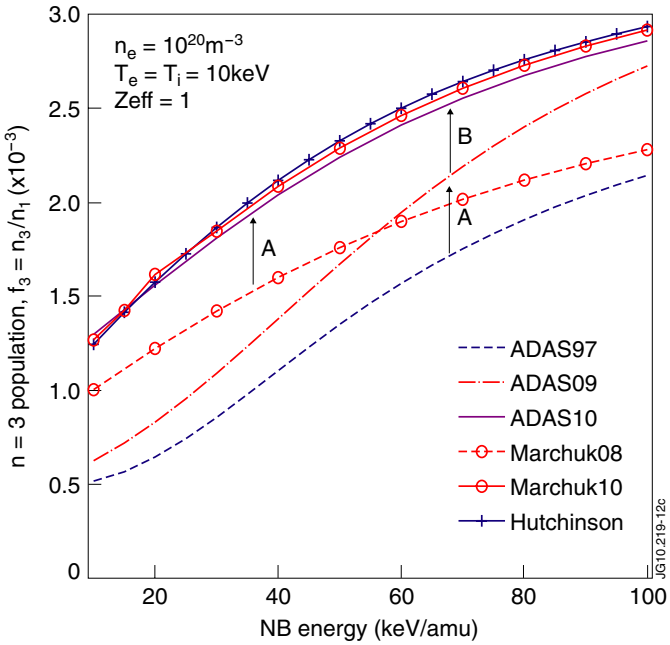

Figure 2. $n = 3$ population in the beam with regard to the ground state according to different CR models. ADAS: ADAS excited beam population [1, 28]; Marchuk: $n = 3$ population from Marchuk *et al* [3]; Hutchinson: excited population digitized from figure 3 in Hutchinson [2]. A denotes the change due to the correction of H($n > 1$) ionization, B marks the change due to a correction of H($n > 1$) CX in ADAS.

only have a modest impact on beam stopping. It is the accuracy of the fundamental datasets concerning the ground state that determines the overall accuracy of the beam stopping cross sections. The quality of proton impact ionization from the ground state is classified in category B by the IAEA [26] and CX with low-Z ions is categorized as B–C (B: uncertainty 10–25%, C: 25–50%). CX is dominant below 40 keV/amu and ion impact ionization above 40 keV/amu. Since Janev and Smith's review on atomic data for fusion plasmas in 1993 [21], there has been remarkable progress in theory concerning these cross sections. The newly published CX cross sections appear to be consistent with the recommended data, but discrepancies have been published for ionization in the intermediate energy region (30–150 keV/amu). In figure 4(*a*) the ion impact ionization cross sections from several authors [29–32] are plotted in comparison with the recommended data [21]. These new data lie higher by about 30% at the peak in the cross section. The Janev and Smith 1993 [21] parametrization at the cross section peak is mostly fitted to the experimental data from Shah *et al* [33, 34]. Initially this agreed with close coupling theory, but it was later shown that these results were not converged [31]. Figure 4(*b*) shows the effect if these increased cross sections would be implemented in the CR beam model. The beam stopping cross section is enhanced by approximately 10% for a typical positive ion source NB operating at 50 keV/amu. Until confirmation of these theoretical results, we have in this publication used the recommended fundamental cross sections for beam stopping for the comparison between measured NB densities from beam emission and modelled beam densities. We have also found no experimental evidence in our data that the current beam stopping cross sections would be too low. Note that this issue does not affect the beam emission rates, it only affects the attenuation of the beam in the modelled beam density that is used as comparison.

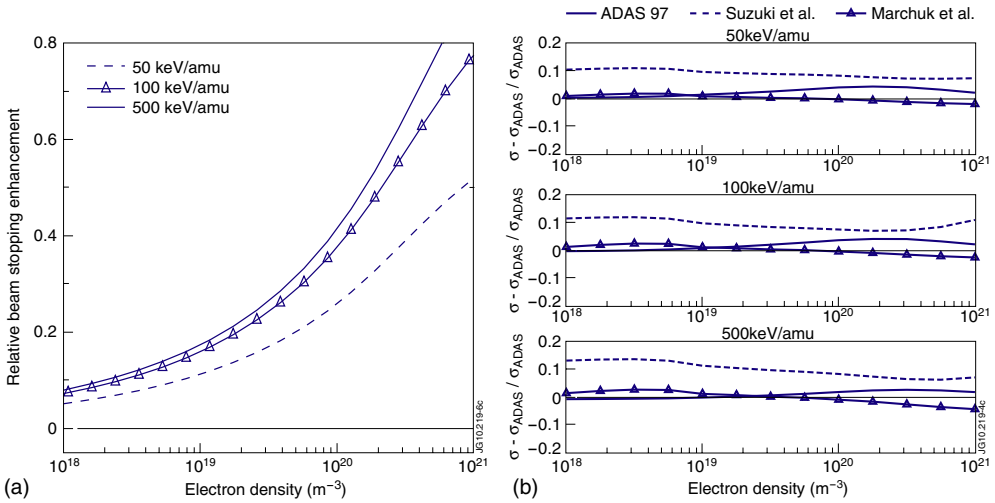

Figure 3. The role of excited states in NB stopping and consistency of beam stopping cross sections from several models. (*a*) Relative increase in the beam stopping cross section due to stepwise ionization trough excited states as a function of electron density, using the CR model of Marchuk *et al* [3]. ($T_e = T_i = 5$ keV, $Z_{eff} = 1$). (*b*) Comparison of NB stopping cross sections from several CR models for the NB. The difference due to the correction of the excited state ionization and CX is also shown. ($T_e = T_i = 5$ keV, $Z_{eff} = 1$).

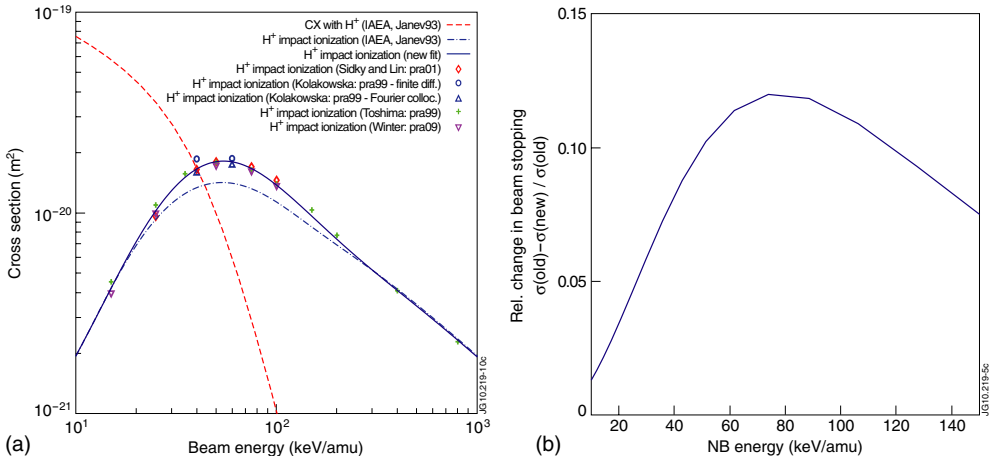

Figure 4. Recent theoretical results on the cross sections for H^+ impact ionization and CX of H(1s), and the impact on the effective beam stopping cross sections. (*a*) Recommended data for ionization and CX compared with data from recent theoretical publications [29–32]. (*b*) Impact of the change in ion impact ionization on the NB stopping cross section. ($T_e = T_i = 5$ keV, $Z_{eff} = 1$).

For JET (50keV/amu) the beam density at the magnetic axis would typically be lowered by 15%, this effect increases to 50% for the ITER diagnostic beam (100 keV/amu).

2.4. CR models for the NB (nkm-resolved)

In the models described above a statistical population among the Stark states within the same *n*-shell was assumed. The violation of this assumption has clearly been demonstrated on

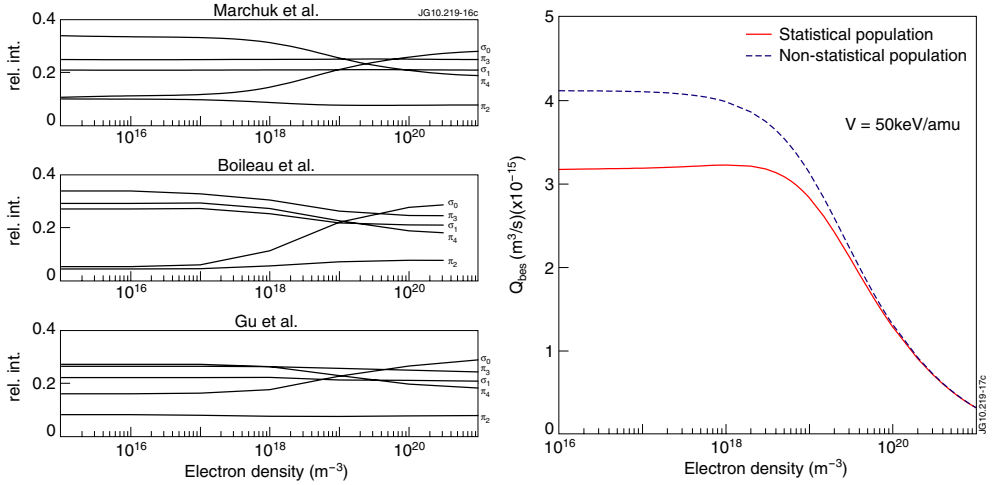

Figure 5. Effect of Stark level resolved modelling on the MSE line ratios and on the total H_α beam emission rate. (*a*) Line ratios within the MSE mulitplet from several Stark resolved CR models [4, 8, 35]. (*b*) Comparison of the H_α beam emission rate for the (*nkm*)- and *n*-resolved CR model of Marchuk *et al* [4] (restricted to $n = 5$, $V = 50$ keV/amu, $T_e = T_i = 5$ keV).

JET [9] and it affects the MSE line ratios and σ/π intensity ratio. Boileau *et al* [8] included all parabolic states into the ADAS CR model up to $n = 4$, extending the model with statistically populated levels at higher n. Excitation cross sections between parabolic states (derived from (nlm)-resolved cross sections) are not available in the literature and therefore these cross sections were calculated in the first Born approximation (B1). Gu *et al* [35] repeated this modelling up to $n = 5$ for use in MSE diagnostic modelling, but their B1 cross sections deviate from those calculated by Boileau *et al*. The validity of B1 cross sections at the intermediate beam energies (≈50 keV/amu) used in current experiments is questionable (see, e.g. [36, p 258]). Marchuk *et al* [4] have calculated the (de)excitation cross sections between all parabolic states in Glauber approximation up to $n = 10$ and implemented these in the NOMAD CR code [37]. For ionization and CX, no (km)-dependence of the donor atom is assumed and the recommended data [21, with corrected ionization] has been used. The results show a significant deviation of the Stark line ratios with regard to the statistical expectation. A strong dependence on the angle between the direction of the collisions and the electric field is found. In figure 5(*a*) the line ratios within the MSE mulitplet are plotted for the three published Stark resolved CR models [4, 8, 35]. Figure 5(*b*) shows the total Balmer-α emission rate compared with the same model enforcing a statistical population (restricted to $n = 5$, $T_e = T_i = 5$ keV and beam voltage is 50 keV/amu). The difference is small at the densities used in current tokamak experiments. The time the beam needs to reach a steady-state population with regard to the ground state is not significantly altered compared with the model that assumes a statistical population (max. 3 cm at 50 keV/amu for $n = 3$). The MSE line ratios and σ/π intensity ratio will be compared with data from JET in section 4.

3. Measured versus predicted beam emission intensity

3.1. Consistency of D_α and D_β beam emission intensities

Beam emission spectra on JET can be recorded along the lines of sight (l.o.s.) of the core CXRS diagnostic [38] on either the blue or red shifted wing of the unshifted D_α peak, depending on

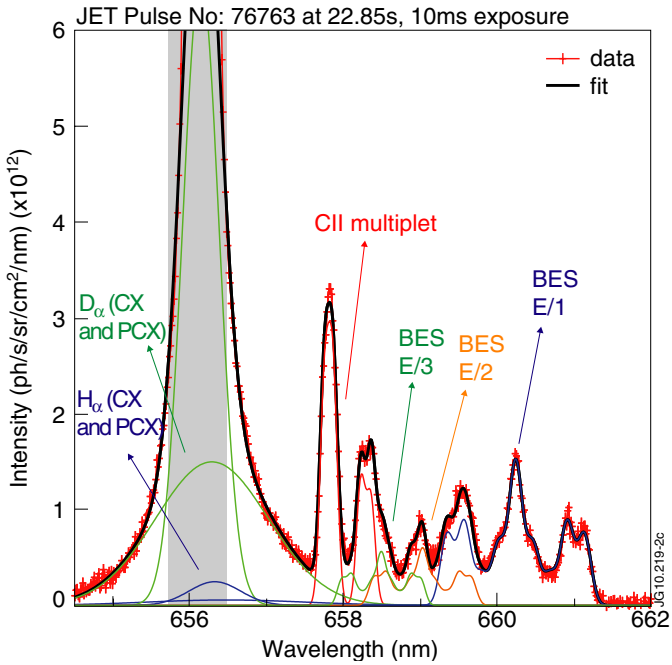

Figure 6. Dα spectrum from JET, the experimental data are marked with crosses, other lines are fitted features. The three energy components of the BES spectrum are indicated. The active and passive D/H CX contributions are approximated as Gaussian lines. The coldest part of the Dα/Hα spectrum (the grey area) is usually overexposed and is neglected in the fit.

which viewing geometry is used. In figure 6(*a*) D_α BES is shown and figure 7 shows a D_β spectrum. The beam emission features of several beams sometimes overlap and can only be distinguished if either the beam voltage is different or if beams from different beam banks ('normal' or 'tangential' [15]) are used. The spectra shown here originate from a pulse where only one beam effectively contributed. A fitting code has been developed to process the full D_α or D_β spectrum, including the beam driven D I CX contribution and the parasitic C II Zeeman multiplet around 6580 Å. The results of the fit are also shown in figures 6 and 7. The ion temperature and plasma rotation derived from the D I CX components is in reasonable agreement with the ion temperature and rotation measured on C VI CX, although no extensive comparison has been made.

In order to compare the measured beam emission intensities with the expected beam densities, the NB attenuation code CHEAP (CHarge Exchange Analysis Package) has been used. The measured beam intensities are converted to the local beam densities integrated along a l.o.s. using the ADAS10 effective emission rates, and the same quantity is obtained from CHEAP using the known intersections between the l.o.s. and the NB. In figure 8, timetraces of the line integrated NB density (full energy fraction) are shown from both beam emission and from the NB attenuation code. Figure 9(*a*) shows a radial profile of the NB density for all three energy fractions in the beam. The measured (labelled 'BES') and expected beam densities (labelled 'BMS') show qualitatively the same behaviour, but they differ by a constant factor. There is a larger deviation on the track closest to the edge. This latter observation was also made by Mandl *et al* [9] and Boileau *et al* [8]. This deviation increases at lower electron density and could qualitatively be attributed to the inappropriate use of steady-state

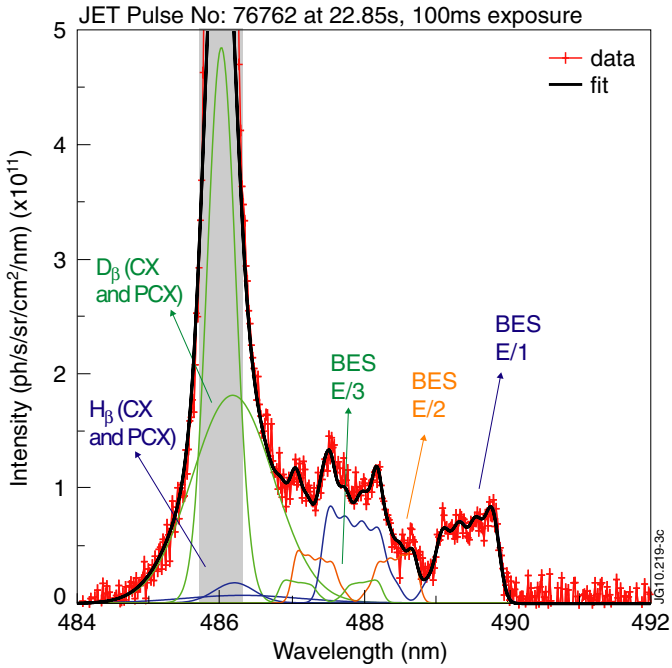

Figure 7. Example Dβ spectrum from JET. The coldest part of the Dβ/Hβ spectrum (the grey area) is neglected in the fit.

emission rates in this region of the plasma where a large electron density gradient exists. We have applied time dependent CR modelling but this did not entirely explain the observations, unless an inaccuracy in the localization of the measurement or the local electron density was assumed as well.

A comparison of the beam densities measured on D_β and D_α BES, respectively, yields an accurate check on the modelled $n = 4$ to $n = 3$ population in the beam. The D_β emission rate is approximately a factor 10 lower than the D_α emission rate. Nevertheless, the measured beam densities agree very well using the ADAS10 emission rates. This is illustrated in figure 9(*b*) on two consecutive, nearly identical shots, once with the spectrometer tuned to D_α BES, once to D_β. The measured densities agree within approximately 10%, most of the difference is correlated with noise on the LIDAR electron density profile. Note that a relatively large discrepancy was found using the outdated emission rates.

As mentioned before, the BES and CHEAP line integrated beam densities agree very well except for a general scaling factor. In figure 10 the measured beam density is plotted against the modelled density for the full energy component in the NB. The measured beam density is 34% lower than expected for beam 8.7 [15]. Apart from the issues related to the atomic modelling of the excited states addressed in this paper, this remaining discrepancy could also be due to inaccuracies in the assessment of the intensity calibration and the geometry between l.o.s. and NB.

The calibration and alignment with the beams is described in detail by Giroud *et al* [15]. The optics are calibrated with an absolutely calibrated source, except for the last window which is calibrated by sending a laser to a retroreflector inside the tokamak vessel. The alignment between the l.o.s. and the NBs is based on beam emission Doppler shifts and relative

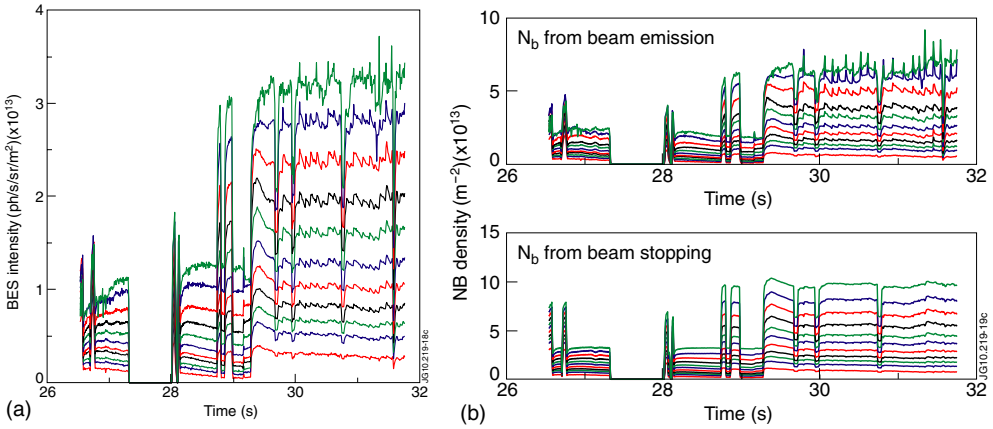

Figure 8. Time traces of the beam emission intensity and the beam density along a line of sight (E/1 component beam 8.7+8.8). The central electron density during the experiment is (4–5.5) $\times 10^{19}$ m^{-3} and $Z_{\rm eff}$ ranges from 1.1 to 1.7 (from Bremsstrahlung). (*a*) Beam emission intensity of the full energy component for #72324 along several l.o.s. of the JET core CXRS diagnostic. Two beams contribute to the BES. (*b*) Time traces of the line integrated NB density (E/1 component) derived from beam emission (top) and from a NB attenuation code (bottom) for #72324. Two beams contribute to the line integrated beam density.

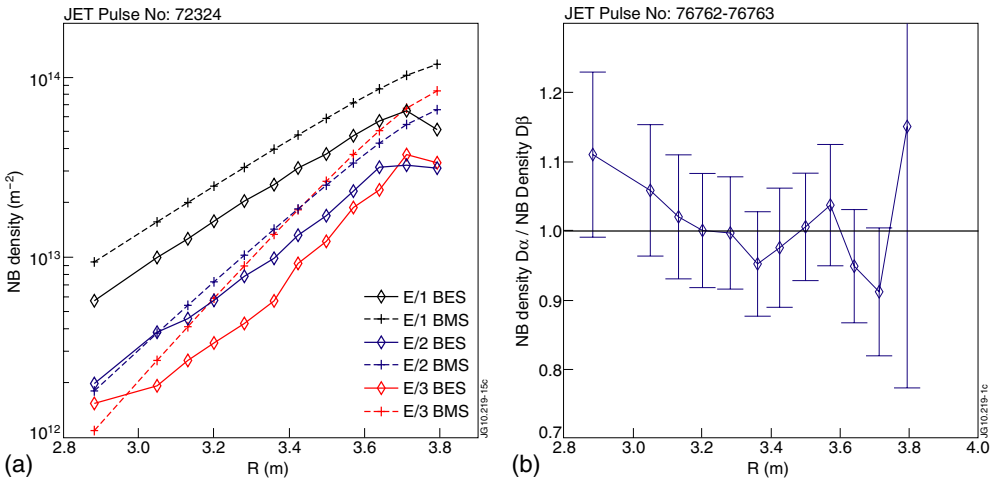

Figure 9. Consistency between beam densities from beam emission and the expected NB density from a beam attenuation code (#72324) and consistency between D_α and D_β. (*a*) Profile of the NB density integrated along a l.o.s. for the three energy fractions in the beam for #72324 at 30.3 s. 'BES' refers to measured data using beam emission, 'BMS' is the expectation from a beam stopping code. (*b*) Ratio of NB densities measured on D_α and D_β beam emission from two similar discharges. The NB attenuation code predicts a maximum difference between the shots of approximately 5% at this time frame. The beam density measured on D_α is consistent with the beam density measured on D_β.

CX intensities when individual beams are switched on/off. The anticipated accuracy of the calibration factor is 6–20% (see [15] for details).

The uncertainty on the active volume is as low as 2% [15], but only if the NB path can be assumed to be perfectly characterized. The characterization of the beam path is

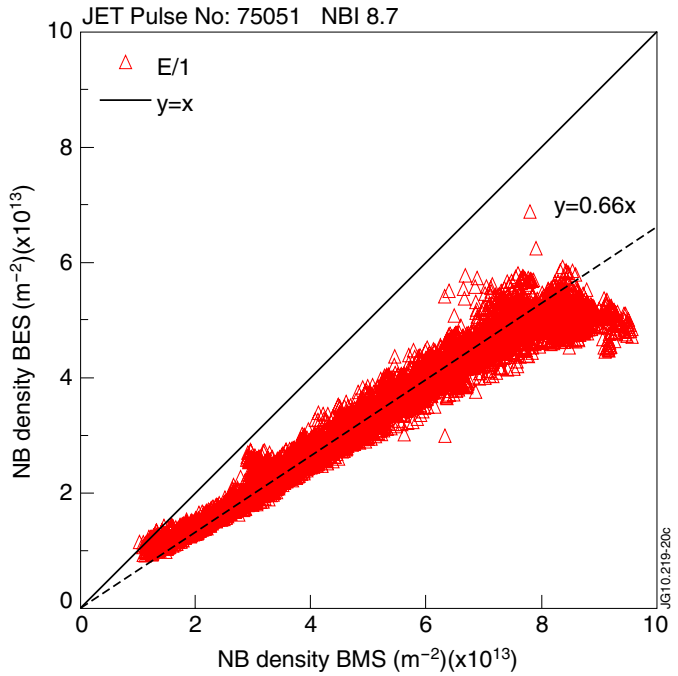

Figure 10. NB density from BES against the beam stopping (BMS) prediction for beam 8.7 (#75051). The odd edge channel is neglected. $n_e(0) = (4.5–5.5) \times 10^{19}$ m^{-3} and $Z_{\text{eff}} = 1.5–2$.

the main source of uncertainty in the determination of the active volumes. The model used to obtain the path length through the beam assumes a diverging Gaussian beam, which is a fair approximation far enough from the beam source, as demonstrated by the beam trajectory simulation code described in [39], which is benchmarked against the beam position and divergence measured from the beam footprint obtained on a calorimeter plate in the NB box [39].

The presence of impurity ions affects both the beam stopping and emission rates. The C^{6+} concentration from CXRS has been taken into account in the evaluation of both the beam stopping and the beam emission rates, neglecting other impurities. Beam stopping is, at 50 keV/amu, a weak increasing function of Z_{eff}, while the beam emission rates decrease with increasing the impurity concentration. However, for the discharges studied here, Z_{eff} from Bremsstrahlung was below 2 and a unreasonably large carbon concentration should be assumed to change the measured beam density by 30%.

The attenuation of the NB and hence the NB power deposition is mainly a function of electron density. The ratio between expected and measured beam densities along a core track as a function of integrated electron density along the NB path gives a calibration independent verification of the beam stopping. Within the range of electron densities for which we have beam emission data, we have seen no trend in the ratio of BES to CHEAP full energy beam densities as a function of electron density. This gives confidence in the effective beam stopping cross sections that are currently in use, although the range of attenuation factors obtained on a single core track was too small to resolve the issue concerning H(1s) ionization by proton impact mentioned in section 2.3.

3.2. NB power fractions from beam emission

Following the methodology of section 3.1, the beam in plasma emission can be used to characterize the distribution of the beam power over the partial energy fractions in the beam (see, e.g., Mandl *et al* [9] for an earlier application of this method). The results of this analysis have been compared with the power fractions based on measurements on the JET Neutral Beam Test Bed and measured by beam into gas emission firing the NB into the tokamak vessel filled with D_2 gas at low pressure. The JET NB Test Bed does not have a bending magnet to remove ions from the partially neutralized beam leaving the neutralizer and therefore the test bed analysis is based on the interpretation of beam emission from a mixed beam of ions and neutrals fired onto a gas target. It requires extensive modelling [40, 41] to interpret the spectroscopic data from the test bed in terms of the power fractions in the ion beam leaving the source. This is then modelled forward in order to obtain the power fractions in the neutralized beam. The comparison with the beam in plasma power fractions revealed a misinterpretation of the spectroscopic data on the NB Test Bed as it is described in [40] and [41] (the beam density in equation (2) in [41] should be beam particle flux, therefore the power in the E/2 and E/3 fractions were underestimated by $\sqrt{2}$ and $\sqrt{3}$, respectively). This error has been corrected and the result of the comparison with beam in plasma emission is shown in figure 11(*a*) for a beam voltage scan. Figure 11(*b*) shows the comparison for a series of beam into gas discharges on JET. After correction of the test bed power fractions and the beam emission rates, all three methods agree rather well.

For the beam into gas discharges of figure 11(*b*), the agreement at the highest and lowest voltage is very good, but a slight discrepancy is seen between 40 and 50 kV/amu. Experimentally determined H_α emission cross sections from Williams *et al* [42] have been used for both the NB into gas power fractions shown here and for the test bed analysis where the emission originates from both the excitation of the neutrals and CX of the ions. The excitation cross sections of atomic hydrogen in H_2 have larger error bars than the H^+ CX cross sections in H_2 [42]. This puts in doubt the reliability of NB into gas experiments for measurement of the NB species mix, despite the more extensive modelling that is required when the power fractions are measured on the ion beam on the test bed or on the NB during standard tokamak operation. The good agreement which is obtained here between the NB in plasma power fractions and the test bed data gives not only some confidence in the voltage scaling of the emission rates between 10 and 55 keV/amu, but it also indicates that beam into plasma emission is a reliable method to obtain the NB species mix *in situ*.

4. Relative intensities within the MSE multiplet

The MSE multiplet on JET is sufficiently resolved on the core channels of the CXRS diagnostic to observe the individual lines of the full energy component. Therefore the measured line intensities can be used to check the modelled Stark level population within $n = 3$. Because the σ-lines are polarized perpendicular to the Lorenz field and the π-line parallel, the observed intensities between σ- and π-lines can be distorted if the front end optics are sensitive to the polarization. Therefore only the ratio of the lines within one polarization group provides a direct comparison which is free from geometric or diagnostic artefacts. Figure 12 shows the measured and predicted MSE line ratios as a function of electron density. Although the minimum electron density that was obtained, is not low enough to do an accurate check on the electron density scaling, the agreement with the modelled line ratios that were obtained with Marchuk *et al*'s CR model [4] is very good and the deviation with the statistical line ratios is clear.

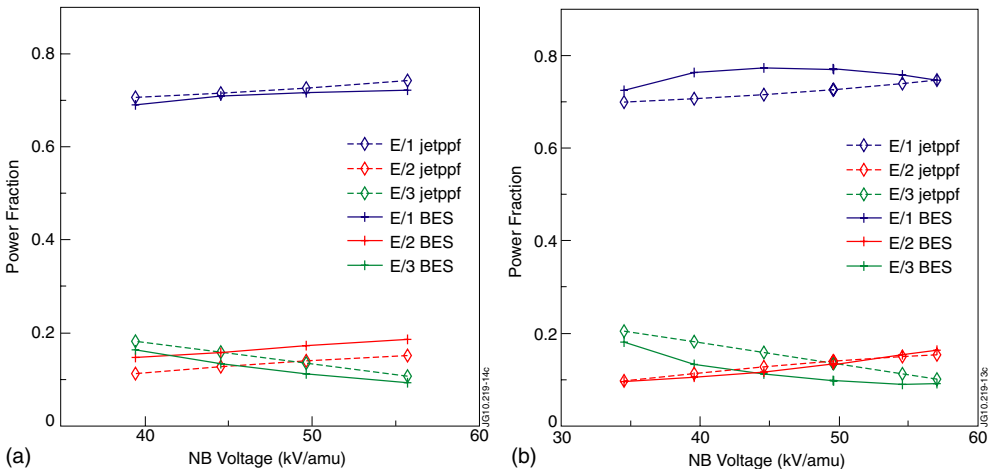

Figure 11. Distribution of the power among the fractional energy components in the NB, as a function of beam voltage. The power fractions measured with beam emission are compared with the expected fractions from a model based on test bed measurements. (*a*) The data labelled 'BES' are from beam emission in plasma (#75046-75050), the data labelled 'jetppf' show the expected power fractions. (*b*) The data labelled 'BES' are from beam in gas emission (#77528-77534), the data labelled 'jetppf' show the expected power fractions.

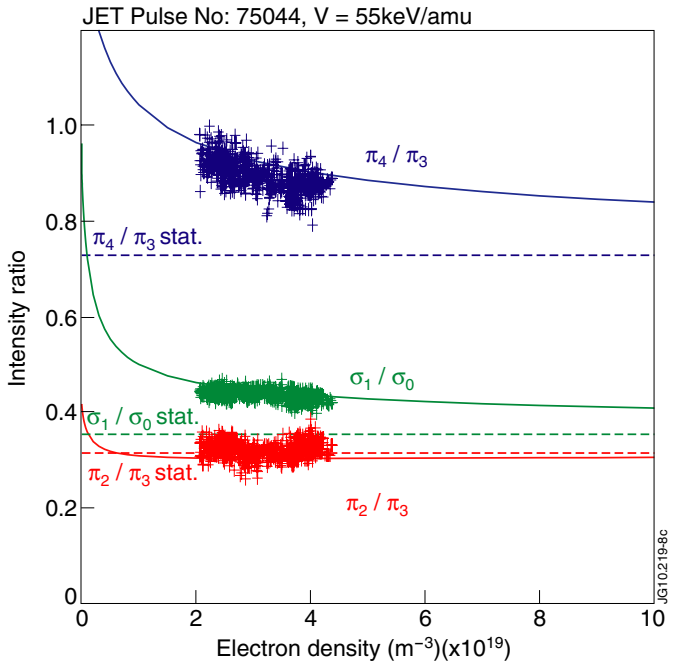

Figure 12. Stark line ratios within the MSE multiplet as a function of electron density. Data from a central track of the JET core CXRS diagnostic (MSE multiplet best resolved) are compared with the model from Marchuk *et al* [4]. The dashed lines show the expected line ratios when the $n = 3$ level would have a statistical subpopulation.

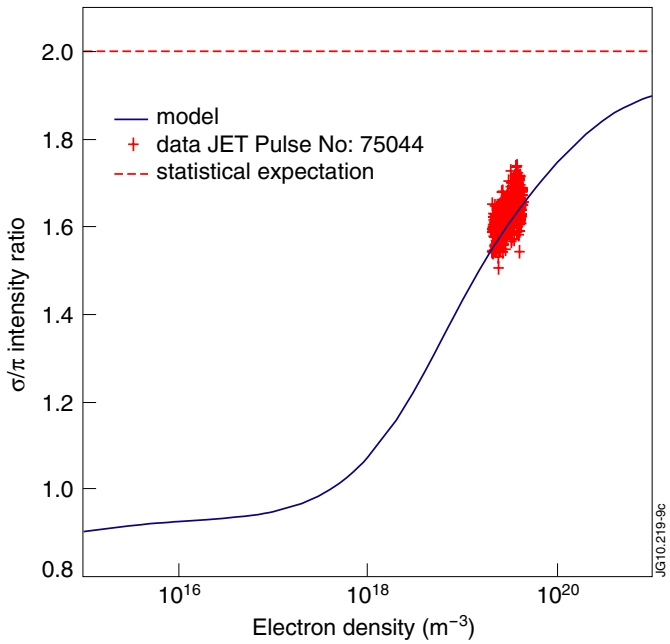

Figure 13. Ratio between the total σ- and π-emissivity (integrated over all solid angles). The experimental data points have been obtained from the measured σ- and π-radiances through $(I_\sigma/I_\pi) = (\Phi_\sigma/\Phi_\pi)/(\Phi_{\sigma 1}A_{\pi 3}/\Phi_{\pi 3}A_{\sigma 1})$. The label 'model' refers to the model of Marchuk *et al* [4]. The dashed line shows the statistical prediction $I_\sigma = 2I_\pi$.

The use of the ratio between the observed σ and π radiance to obtain information on the direction of the Lorenz field, and hence on the magnetic pitch angle, has rarely been successful. This is mainly due to the non-statistical features in the MSE spectrum. The classical polarization based MSE diagnostic [43] is much less sensitive to this effect, except when σ and π lines overlap in the sampled wavelength region. In this case a change in electron density could change the amount of σ and π light which is sampled. In figure 13 the modelled total σ- and π-emissivity is plotted as a function of electron density for a beam energy of 55 keV/amu. The difference with the statistically expected ratio can be as high as 20% for standard tokamak conditions. In order to compare with the experimentally observed ratio, the disturbing effect of the geometry and the polarization sensitivity of the first mirror was obtained using the ratio between the $\sigma 1$- and $\pi 3$-lines. These originate from the same upper level and hence $\Phi_{\sigma 1}/\Phi_{\pi 3}$ is independent of the population structure. However, because the Stark splitting is usually not large enough, it is in practical situations difficult to obtain this ratio with the accuracy that is needed for direct use as a constraint on the magnetic field reconstruction. The measurements compare well with the model, but the use of $\Phi_{\sigma 1}$ and $\Phi_{\pi 3}$ induces considerable statistical noise.

In figure 14, the expected measurement Φ_σ/Φ_π is plotted as a function of the angle θ between a line of sight and the Lorentz field taking into account the effects of the $n = 3$ non-statistical population and a first mirror with an s-reflectivity which is 15% larger than the p-reflectivity. This value was obtained from the $\Phi_{\sigma 1}/\Phi_{\pi 3}$ ratio and the known beam and l.o.s. geometry during a beam into gas shot for which the magnetic field is purely toroidal. One can see that the main effect that causes a deviation between the simple geometrical prediction $(\Phi_\sigma/\Phi_\pi = (1 + \cos^2\theta)/\sin^2\theta)$ and the measurements is the non-statistical character of the

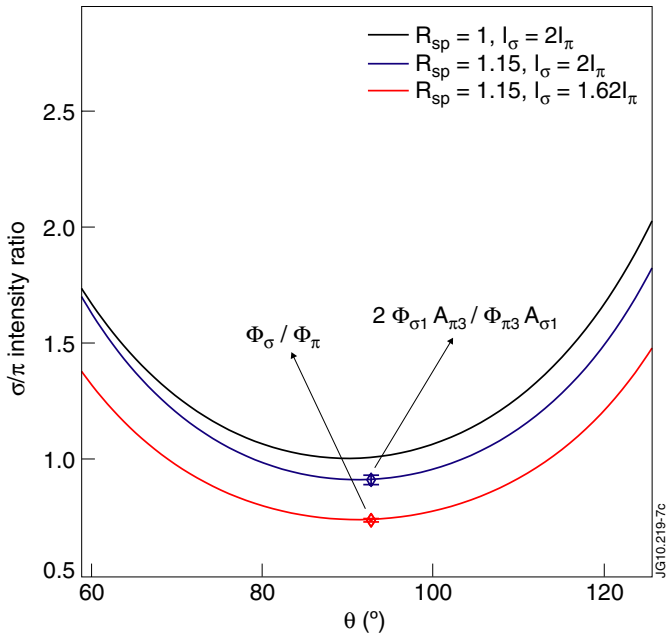

Figure 14. Ratio of the expected σ- over π-radiance as a function of angle θ between a core line of sight and the Lorentz field. $R_{\rm sp}$ is the ratio between the s-and p-reflectivity of the first mirror. The case $R_{\rm sp} = 1$, $I_\sigma = 2I_\pi$ corresponds to the standard prediction $\Phi_\sigma/\Phi_\pi = (1 + \cos^2\theta)/\sin^2\theta$. The two curves below correspond to the situation with a polarization sensitive first mirror and with a $n = 3$ population that has not reached a statistical distribution. The points indicate measurements from JET #75044. For this viewing geometry a large change in θ is needed to cause an appreciable change in the measured Φ_σ/Φ_π intensity ratio.

$n = 3$ population. The measured points agree very well with the modelled curves, however, for the equatorial viewing geometry used here, this method cannot be used to obtain useful information about θ (and hence the magnetic pitch angle), because a large change in θ is needed to cause a measurable change in Φ_σ/Φ_π.

5. Conclusions

In this paper we have analysed the consistency of several CR models [1–3] that have been developed to calculate the NB stopping and population of excited states in hydrogen plasmas. The results of the calculations are compared with experimental data from JET. Revisiting the proton impact ionization of excited states and identification of a mistake in the ADAS rescaling of the charge exchange cross sections allowed us to achieve consistency between all models. The corrected data will be in a next ADAS release. The calculated relative $n = 3$ to $n = 4$ population agrees within 10% to the measured ratio from JET using the H_α to H_β beam emission intensities. Good agreement is found as well on the power fractions measured with BES and on the JET Neutral Beam Test Bed, if a correction to the analysis in [40, 41] is taken into account. The power fractions measured with NB in gas emission show a slightly larger deviation. The radial profiles and time traces of the measured and modelled NB density agree well but the overall intensity of the measured beam density is $\approx$30% lower. The reason for this is uncertain. Apart from the involved atomic data, this could also be due to a combination

of calibration, alignment and especially the characterization of the NB path. These issues are currently the main motivation to use beam emission. The Stark line intensities within the MSE multiplet are in good agreement with a sublevel resolved model [4]. The measured σ/π intensity is disturbed by the polarization characteristics of the tokamak side optics and the $n = 3$ subpopulation structure, the latter effect is consistent with the CR modelling.

The overall agreement found on JET between the modelled and expected beam emission intensities gives confidence in the proposed scheme combining charge exchange and beam emission that will be used to measure the helium ash on ITER. The agreement between the modelled and measured MSE spectra gives confidence in the Stark resolved CR modelling and hence such a model could be used to correct the measured σ/π-ratio when used to constrain magnetic field reconstructions.

Acknowledgments

This work was supported by EURATOM and carried out within the framework of the European Fusion Development Agreement. The views and opinions expressed herein do not necessarily reflect those of the European Commission.

References

[1] Anderson H, von Hellermann M G, Hoekstra R, Horton L D, Howman A C, Konig R W T, Martin R, Olson R E and Summers H P 2000 *Plasma Phys. Control. Fusion* **42** 781–806
[2] Hutchinson I H 2002 *Plasma Phys. Control. Fusion* **44** 71–82
[3] Marchuk O, Bertschinger G, Biel W, Delabie E, von Hellermann M G, Jaspers R and Reiter D 2008 *Rev. Sci. Instrum.* **79** 10F532
[4] Marchuk O, Ralchenko Yu, Janev R K, Biel W, Delabie E and Urnov A M 2010 *J. Phys. B: At. Mol. Opt. Phys.* **43** 011002
[5] Janev R K, Boley C D and Post D E 1989 *Nucl. Fusion* **29** 2125–40
[6] Suzuki S, Shirai T, Nemoto M, Tobita K, Kubo H, Sugie T, Sakasai A and Kusama Y 1998 *Plasma Phys. Control. Fusion* **40** 2097–111
[7] Seraydarian R P, Burrell K H and Groebner R J 1988 *Rev. Sci. Instrum.* **59** 1530–2
[8] Boileau A, Von Hellermann M, Horton L D, Spence J and Summers H P 1989 *Plasma Phys. Control. Fusion* **31** 779–804
[9] Mandl W, Wolf R C, von Hellermann M G and Summers H P 1993 *Plasma Phys. Control. Fusion* **35** 1373–94
[10] von Hellermann M G, Jaspers R J E, Summers H P and Zastrow K-D 2001 *Advanced Diagnostics for Magnetic and Inertial Fusion* ed P Stott *et al* (New York: Kluwer) pp 125–8
[11] De Bock M, Jakubowska K, von Hellermann M G, Jaspers R J E, Donne A J H and Shmaenok L 2004 *Rev. Sci. Instrum.* **75** 4155–7
[12] Jaspers R J E, von Hellermann M G, Delabie E, Biel W, Marchuk O and Yao L 2008 *Rev. Sci. Instrum.* **79** 10F526
[13] Rowan W L, Sampsell M B and Granetz R S 2004 *Rev. Sci. Instrum.* **75** 3487–9
[14] Euringer H and Verplancke Ph 1994 *Rev. Sci. Instrum.* **65** 2996–9
[15] Giroud C, Meigs A G, Negus C R, Zastrow K D, Biewer T M, Versloot T W and JET-EFDA Contributors 2008 *Rev. Sci. Instrum.* **79** 10F525
[16] Jakubowska K, De Bock M, Jaspers R, Von Hellermann M and Shmaenok L 2004 *Rev. Sci. Instrum.* **75** 3475–7
[17] Pablant N A, Burrell K H, Groebner R J, Kaplan D H and Holcomb C T 2008 *Rev. Sci. Instrum.* **79** 10F517
[18] Wolf R C, Eriksson L-G, Von Hellermann M, Konig R, Mandl W and Porcelli F 1993 *Nucl. Fusion* **33** 1835
[19] Foley E L, Levinton F M, Yuh H Y and Zakharov L E 2008 *Rev. Sci. Instrum.* **79** 10F521
[20] Boley C D, Janev R K and Post D E 1984 *Phys. Rev. Lett.* **52** 534–7
[21] Janev R K and Smith J 1993 *Atomic Plasma Mater. Int. Data Fusion, Nucl. Fusion* (suppl)
[22] Fainstein P D, Ponce V H and Rivarola R D 1990 *J. Phys. B: At. Mol. Opt. Phys.* **23** 1481–9
[23] Igarashi A and Shirai T 1994 *Phys. Rev.* A **50** 4945–50
[24] McCartney M and Crothers D S F 1995 *Z. Phys. D: Atoms Mol. Clusters* **35** 1–2

[25] Olivera G H, Rivarola R D and Fainstein P D 1995 *Phys. Rev.* A **51** 847–9
[26] ALADDIN database maintained by the IAEA http://www-amdis.iaea.org/aladdin
[27] O'Mullane M http://www.adas.ac.uk/notes/adas_c09-01.pdf
[28] Summers H P 2004 *The ADAS User Manual, version 2.6* http://adas.phys.strath.ac.uk
[29] Emil Y. Sidky and Lin C D 2001 *Phys. Rev.* A **65** 012711
[30] Kołakowska A, Pindzola M S and Schultz D R 1999 *Phys. Rev.* A **59** 3588–91
[31] Toshima N 1999 *Phys. Rev.* A **59** 1981–7
[32] Winter T G 2009 *Phys. Rev.* A **80** 032701
[33] Shah M B and Gilbody H B 1981 *J. Phys. B: At. Mol. Opt. Phys.* **14** 2361–77
[34] Shah M B, Elliott D S and Gilbody H B 1987 *J. Phys. B: At. Mol. Opt. Phys.* **20** 2481–5
[35] Gu M F, Holcomb C T, Jayakuma R J and Allen S L 2008 *J. Phys. B: At. Mol. Opt. Phys.* **41** 095701
[36] Bransden B H and McDowell M R C 1992 *Charge Exchange and the Theory of Ion-Atom Collisions* (Oxford: Clarendon)
[37] Ralchenko Yu and Maron Y 2001 *J. Quant. Spectrosc. Radiat. Transfer* **71** 609–21
[38] Negus C R, Giroud C, Meigs A G, Zastrow K D, Hillis D L and JET-EFDA Contributors 2006 *Rev. Sci. Instrum.* **77** 10F102
[39] Ciric D, Milnes J J and Surrey E 2002 Misalignment on multi-aperture particle beam properties *19th IEEE/NPSS Symp. on Fusion Engineering (Atlantic City, NJ)*
[40] Hemsworth R S 1985 *JET Report* JET-DN-C(85)8
[41] Uhlemann R, Hemsworth R S, Wang G and Euringer H 1993 *Rev. Sci. Instrum.* **64** 974–82
[42] Williams I D, Geddes J and Gilbody H B 1982 *J. Phys. B: At. Mol. Phys.* **15** 1377–89
[43] Levinton F M, Fonck R J, Gammel G M, Kaita R, KugelL H W, Powell E T and Roberts D W 1989 *Phys. Rev. Lett.* **63** 2060–3